On the output frequency measurement within cup anemometer calibrations

Authors:

Alvaro Ramos-Cenzano, Mikel Ogueta-Gutierrez, Santiago Pindado

Instituto Universitario de Microgravedad "Ignacio Da Riva" (IDR/UPM)
ETSI Aeronáutica y del Espacio, Universidad Politécnica de Madrid
Pza. del Cardenal Cisneros 3, Madrid 28040, Spain

e-mail:
santiago.pindado@upm.es (Santiago Pindado)

Keywords:

cup anemometer, anemometer calibration, output frequency, FFT, Thies FirstClass

Abstract:

The output frequency of five commercial anemometers (Thies Clima First-Class Advanced) was studied. The output voltage of these anemometers was measured at the calibrations process at 25 kHz sampling frequency, during 25 seconds. The output frequency was calculated by two different procedures: by Counting Pulses (CP) and by using the Fast Fourier Transform (FFT). The errors of the anemometers' transfer function based on both ways for calculating the output frequency are given in relation to the reference calibration results, obtained with an ISO 17025 standard calibration process. The effect of the sampling frequency and the length of the sample are analyzed. The results of using FFT are compared to the ones resulting from using CP. Counting Pulses (CP) has proven to be the most accurate way to extract the anemometer's output frequency from data recorded.

1 Introduction

Despite the recent developments of sonic anemometers [1–5], nacelle anemometers [6–11], LIDAR and SODAR [12–21], cup anemometer remains the most common wind speed sensor within the wind energy and meteorology sectors.

Furthermore, the trends in the installed wind power even suggest an increase of the massive consumption of these sensors in the upcoming years [22]. Cup anemometers require a thorough calibration process prior installation [23–26], no matter if it is in a meteorology mast or on the top of a wind turbine. Although this wind speed sensor is today the most popular technology within the industrial sectors, it should be also said that it has certain limitations related to the inertial effects of the rotor in turbulent flows (that causes the well-known overspeeding effect) [27–32].

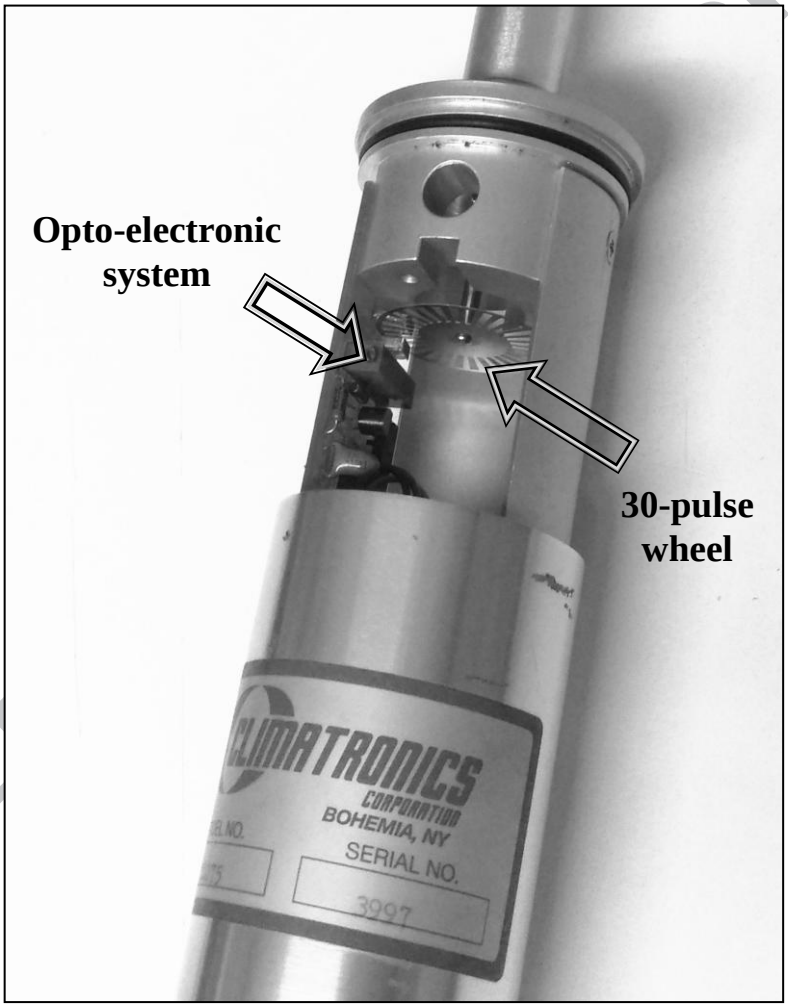

Figure 1. Opto-electronic output signal generator system of the Climatronics 100075 cup anemometer.

In recent works at IDR/UPM Institute, the performance of cup anemometers has been analyzed taking into account the output signal [26,33–35]. The transfer function (also known as calibration curve) of a cup anemometer is defined by the following equation:

$$V = \mathrm{A}\cdot f + \mathrm{B}, \tag{1}$$

in which the wind speed, *V*, is calculated in relation to the output frequency of the anemometer, *f*, the slope and offset (A and B, respectively) being defined by a calibration process (see Section 2 of the present work).

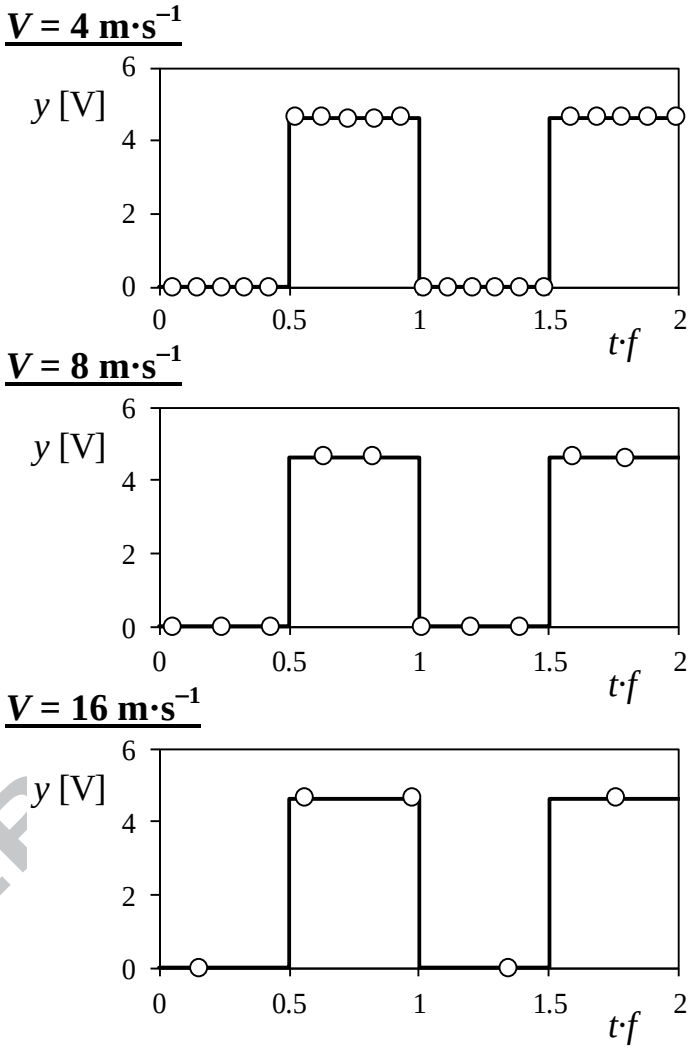

Figure 2. Examples of sampling the analog square-wave output signal of a cup anemometer with same sampling frequency at different wind speeds. The output voltage *y* is plotted in relation to the non-dimensional time *t·f* (where *f* is the anemometer's output frequency). From [35].

The proper calculation of cup anemometers output frequency during their calibration process is of paramount importance. Bearing in mind that normally the most common top-class anemometers (Thies Clima First-Class or Vector Instruments A100 LK/LM) give a square wave signal due to the opto-electronic output signal system (see

an example of this system in Figure 1), it is important to sample adequately the output system in order to extract an accurate value of the aforementioned output frequency. See in Figure 2 the pulses given by a cup anemometer equipped with an opto-electronic output system, and the data obtained at three different wind velocities when this analog signal is measured at 830 Hz sampling frequency. As it can be observed, less measurement points are available to extract the anemometer's output frequency for larger wind-speeds.

In the present work, two methods for extracting the output frequency from a sampled square wave signal, Counting Pulses (CP) and the Fast Fourier Transform (FFT), are compared, the effect of the sampling frequency and the length of the data sample on the cup anemometer transfer function accuracy being also analyzed. This is the main and more important contribution of the work, as many calibration facilities obtain the output frequency by using FFT without being aware of the differences (in terms of accuracy) in relation to CP.

This technical note is organized as follows. In Section 2 the calibration and post-processing process are described. The results are discussed in Section 3, and the conclusions are summarized in Section 4.

2 Testing configuration and cases studied

The calibrations of five Thies Clima First-Class Advanced anemometers are analyzed in this work. The calibrations were performed at LAC-IDR/UPM calibration lab, following MEASNET procedures. More information on this facility and the lab can be found in [23]. In brief, a calibration is a wind-tunnel testing of an anemometer in which a correlation between the output frequency of the instrument and the wind-flow speed is carried out. Thirteen measurement points are taken between 4 $m \cdot s^{-1}$ and 16 $m \cdot s^{-1}$ to stablish that correlation and define the transfer function of the anemometer through the calibration constants A and B, see equation (1). The anemometers calibrated are called hereinafter Anemometer-1 to Anemometer-5, the transfer function obtained during their calibration process being called the reference calibration (hereinafter defined by constants A^* and B^*).

During each point of those calibrations a sample of 25 seconds at 25 kHz was recorded with a National Instruments NI USB-6210 Data Acquisition System. From these data records four new ones with lengths 20, 15, 10, and 5 s were generated for

each anemometer. Additionally, new data sets with different sampling frequencies were obtained extracting selected points from each data sample (e.g., the 1 kHz samples were obtained taking one out of twenty-five points from the original samples). Therefore, 100 different calibration sets were generated for each anemometer in order to analyze: 1) the effects of the sampling frequency, 2) the length of the data sample and 3) the way to extract the output frequency (comparing CP and FFT), on the cup anemometer transfer function. These equations were directly compared to the reference one in order to quantify the accuracy of the calculated transfer function. See in Table 1 a list of the cases analyzed from the recorded data.

Table 1. Cases analyzed in the present work.

Anemometers calibrated	• Anemometer-1 • Anemometer-2 • Anemometer-3 • Anemometer-4 • Anemometer-5	
Points per calibration	• 4 $m \cdot s^{-1}$ • 5 $m \cdot s^{-1}$ • 6 $m \cdot s^{-1}$ • 7 $m \cdot s^{-1}$ • 8 $m \cdot s^{-1}$ • 9 $m \cdot s^{-1}$ • 10 $m \cdot s^{-1}$	• 11 $m \cdot s^{-1}$ • 12 $m \cdot s^{-1}$ • 13 $m \cdot s^{-1}$ • 14 $m \cdot s^{-1}$ • 15 $m \cdot s^{-1}$ • 16 $m \cdot s^{-1}$
Length of samples	• 5 s • 10 s • 15 s • 20 s • 25 s	
Sampling frequencies analyzed	• 500 Hz • 625 Hz • 657.89 Hz • 675.98 Hz • 694.44 Hz • 714.29 Hz • 735.29 Hz • 757.58 Hz • 781.25 Hz • 806.45 Hz	• 833.33 Hz • 862.07 Hz • 892.86 Hz • 925.93 Hz • 961.54 Hz • 1000 Hz • 1250 Hz • 5000 Hz • 12500 Hz • 25000 Hz
Calculation of the output frequency, *f*	• CP (Counting Pulses) • FFT	

3 Results

In Figure 3 the transfer function of the Anemometer-1 reference calibration is plotted (solid line), together with the corresponding points from the Anemometer-1/25-second 500 and 1000 Hz datasets, extracted by CP. It can be observed in the figure that the anemometer output frequencies calculated from the 1000 Hz sampling rate dataset seem quite accurate (as they fit the reference calibration well), whereas the output frequency calculated from the 500 Hz sampling rate dataset presents problems for wind speeds above 11 $m \cdot s^{-1}$. The obvious explanation of this effect lies on the anemometer's output square-wave frequency, which is larger than 250 Hz for those wind speeds. Therefore and according to Nyquist theorem [36], a sampling frequency above 500 Hz is required to extract correctly the output frequency at 12 $m \cdot s^{-1}$ or larger wind velocities. Besides, the transfer function (1) based on the points calculated with the 500 Hz dataset has been also plotted in Figure 3 (dashed line). The poor accuracy of this transfer function in relation to the reference one can be observed in the figure.

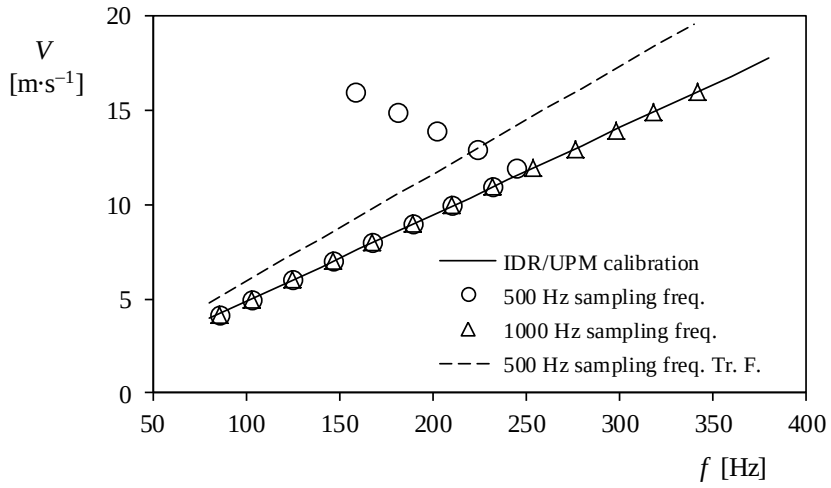

Figure 3. Anemometer-1/25-second 500 and 1000 Hz datasets. Points (output frequencies) extracted by CP. IDR/UPM reference calibration, i.e., transfer function of Anemometer-1 has been included (solid line). The transfer function (Tr. F.) based on the Anemometer-1/25-second 500 Hz dataset is also included (dashed line).

A simple but effective way to estimate the accuracy of a transfer function is by calculating the residuals. The residuals, $r_{s,i}$, in an anemometer calibration are the wind

speed differences between the testing wind speeds, V_i, and the ones from the transfer function at the calculated output frequencies, f_i:

$$r_{s,i} = V_i - \left(\mathrm{A}\cdot f_i + \mathrm{B}\right). \quad (2)$$

In Figure 4, the absolute values of the residuals from the transfer functions based on the Anemometer-1/25-second 500, 625, 675.68, and 1000 Hz datasets calculated by CP are plotted. As expected, smaller residuals are obtained with higher sampling rates.

An alternative way to estimate the accuracy of the calculated transfer functions has been also used in the present work. The wind speed error in relation to the reference transfer function has been calculated for the transfer functions obtained from the different sampling frequency datasets:

$$\Delta V_i = \left(\mathrm{A}^*\cdot f_i + \mathrm{B}^*\right) - \left(\mathrm{A}\cdot f_i + \mathrm{B}\right). \quad (3)$$

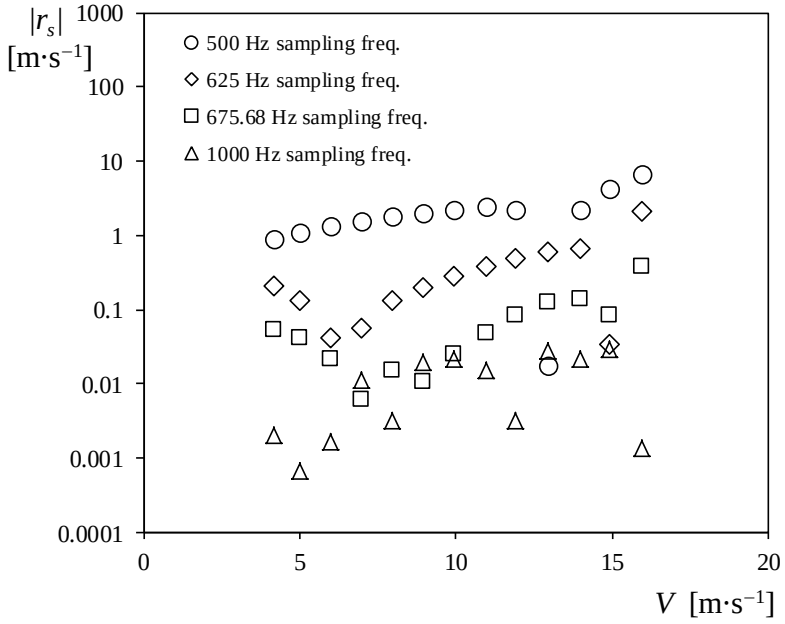

Figure 4. Anemometer-1/25-second 500, 625, 675.68, and 1000 Hz datasets. Absolute values of the transfer functions residuals, r_s, calculated by CP.

In Figure 5, the absolute values of these wind speed differences are plotted for the aforementioned transfer functions calculated by CP with the Anemometer-1/25-seconds 500, 625, 675.68, and 1000 Hz datasets. As expected also, the best results are obtained with higher sampling rates. The wind speed error is three orders of magnitude smaller for a frequency of 1000 Hz than for a frequency of 500 Hz.

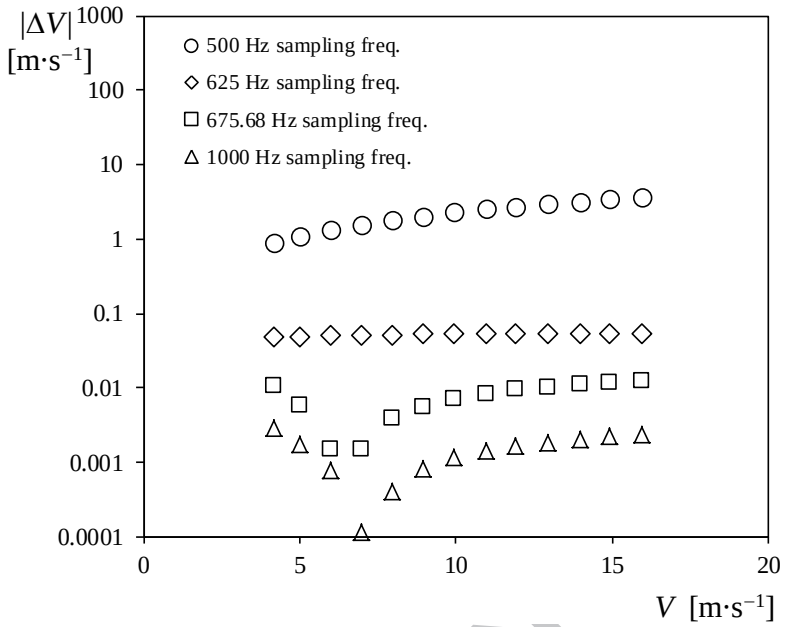

Figure 5. Anemometer-1/25-second 500, 625, 675.68, and 1000 Hz datasets. Absolute values of the wind speed error, ΔV, calculated by CP.

Additionally, an averaged value of the residuals, R_S, and an averaged percentage value of the wind speed error, ΔV_{avg}:

$$R_S = \frac{1}{13}\sum_{i=1}^{13}\left|r_{s,i}\right|, \tag{4}$$

$$\Delta V_{avg} = \frac{1}{13}\sum_{i=1}^{13}\frac{\left|\Delta V_i\right|}{\left(\mathrm{A}^* f_i + \mathrm{B}^*\right)}, \tag{5}$$

have been proposed to characterize the accuracy of the transfer functions corresponding to all analyzed different sampling rate datasets. The values of both parameters corresponding to the Anemometer-1/25-second datasets, extracted both by CP and by using the FFT, are plotted in Figures 6 and 7. In those figures, the left graph displays the results for all the frequencies measured, whereas the right graph is a detailed view of the lower frequencies results (500 Hz to 1000 Hz).

In figure 6 the behavior of the residuals is shown. It is clear that both methods, CP and FFT, reach a constant value once the frequency is increased enough. This constant value is smaller in the case of the CP. However, the frequency at which this value is reached is a bit smaller in the case of the FFT. The same trend can be seen in figure 7, where the averaged percentage values of the wind speed errors are displayed.

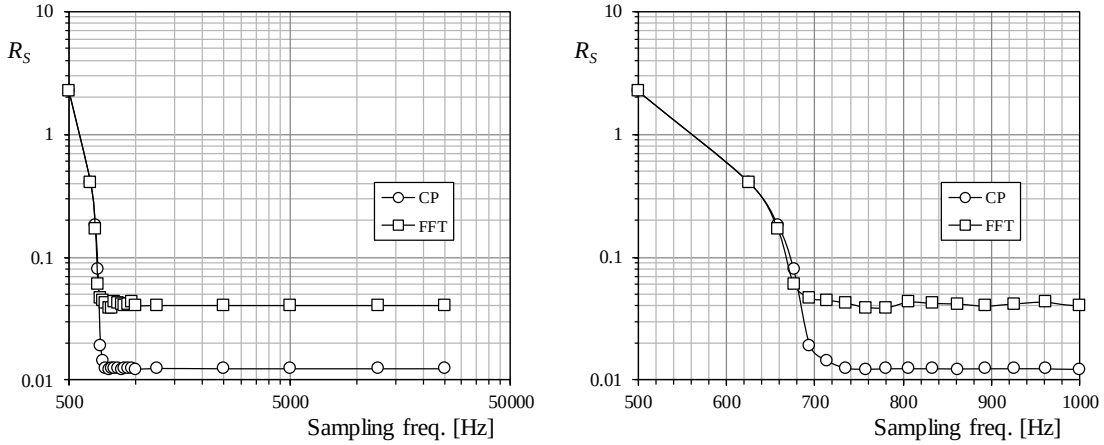

Figure 6. Anemometer-1/25-second datasets. Averaged value of the transfer functions residuals, R_S, in relation to the sampling frequency. The residuals were calculated by CP and by using FFT. On the left, all the results are displayed, whilst on the right, only the results for frequencies from 500 Hz to 1000 Hz are displayed.

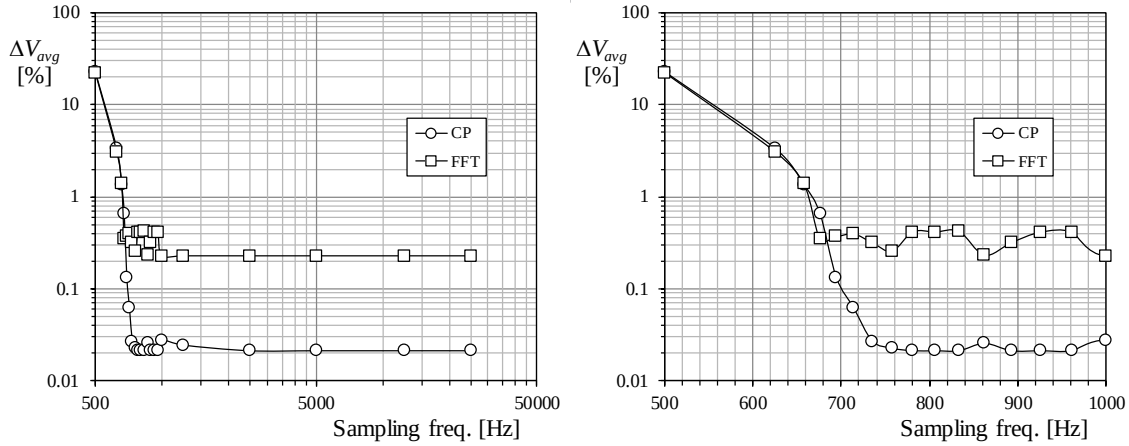

Figure 7. Anemometer-1/25-second datasets. Averaged value of the transfer functions wind speed error, ΔV_{avg}, in relation to the sampling frequency. The residuals were calculated by CP and by using FFT. On the left, all the results are displayed, whilst on the right, only the results for frequencies from 500 Hz to 1000 Hz are displayed.

The effect of the dataset length on the aforementioned stabilized values of the residuals, $R_S|_{st}$, and the wind speed error, $\Delta V_{avg}|_{st}$, is shown in Figures 8 to 12 for the five anemometers studied. The decreasing trends of both parameter in relation to the sampling dataset length is shown in the graphs from these figures, the results obtained by CP being better as they show lower values when compared to the results obtained by using FFT.

Finally, the percentage errors of the calibrations based on the 25kHz/25-second datasets and calculated with FFT, in relation to the reference calibrations, ΔV, are included for Anemometers 1 to 5 in Figure 13. From this results it can be deduced that the error depends on the wind speed (that is, on the output frequency), the relationship between the errors and the variable (wind speed or output frequency) being similar to a first order transfer function. Although, the errors seems to be within ±0.4% bracket, this figure being a first approximation to the uncertainty, it could be quite premature to stablish the contribution of the FFT procedure to the calibration uncertainty, as a whole analysis on the different sources of error would be required.

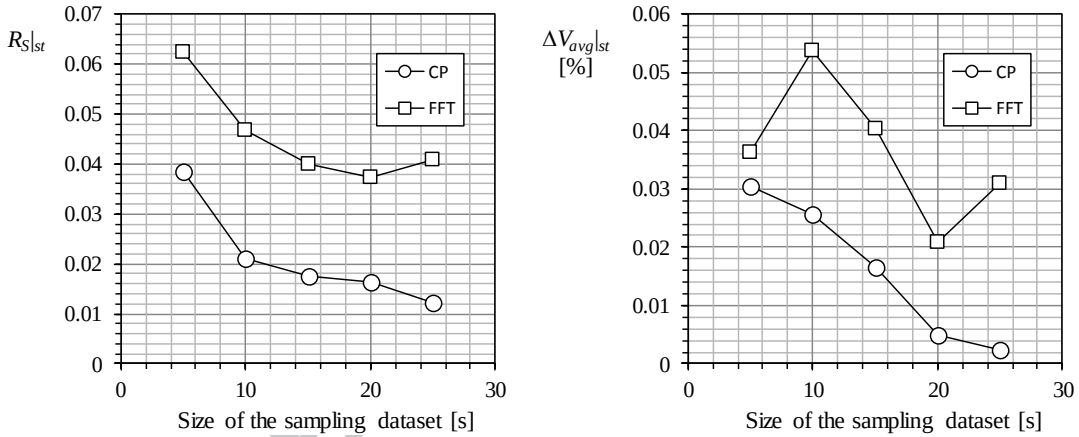

Figure 8. Anemometer-1. Stabilized values of the residuals, $R_S|_{st}$, and the wind speed error, $\Delta V_{avg}|_{st}$, in relation to the sampling dataset length.

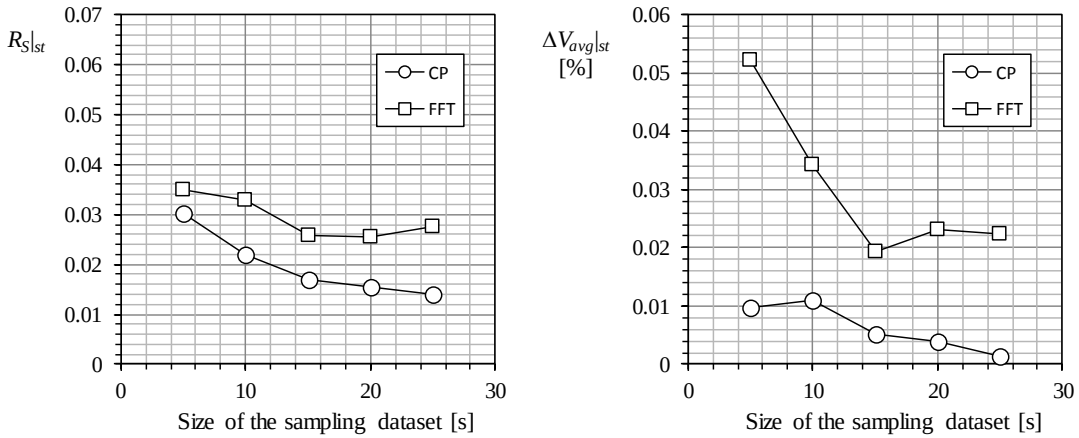

Figure 9. Anemometer-2. Stabilized values of the residuals, $R_S|_{st}$, and the wind speed error, $\Delta V_{avg}|_{st}$, in relation to the sampling dataset length.

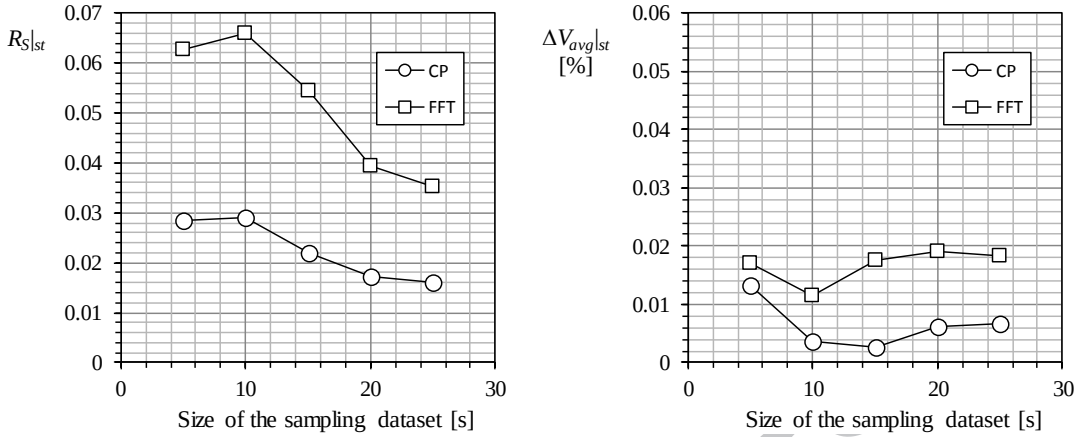

Figure 10. Anemometer-3. Stabilized values of the residuals, $R_S|_{st}$, and the wind speed error, $\Delta V_{avg}|_{st}$, in relation to the sampling dataset length.

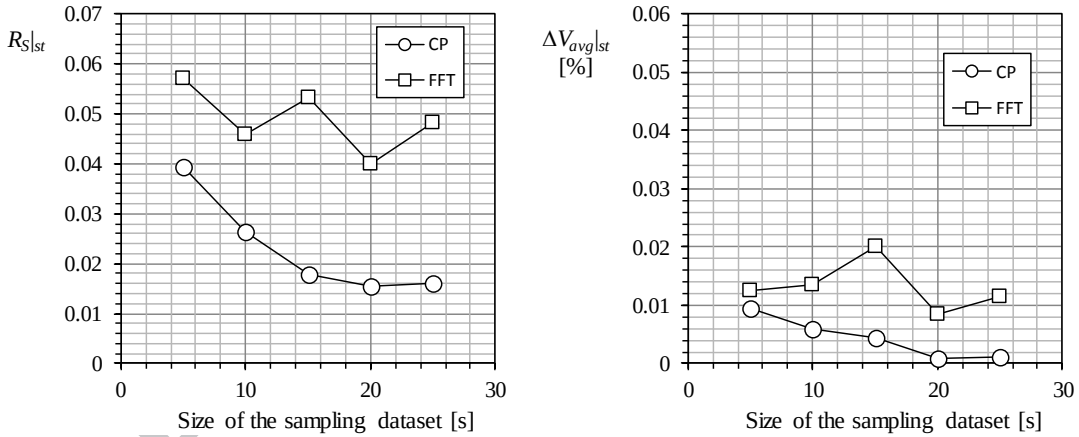

Figure 11. Anemometer-4. Stabilized values of the residuals, $R_S|_{st}$, and the wind speed error, $\Delta V_{avg}|_{st}$, in relation to the sampling dataset length.

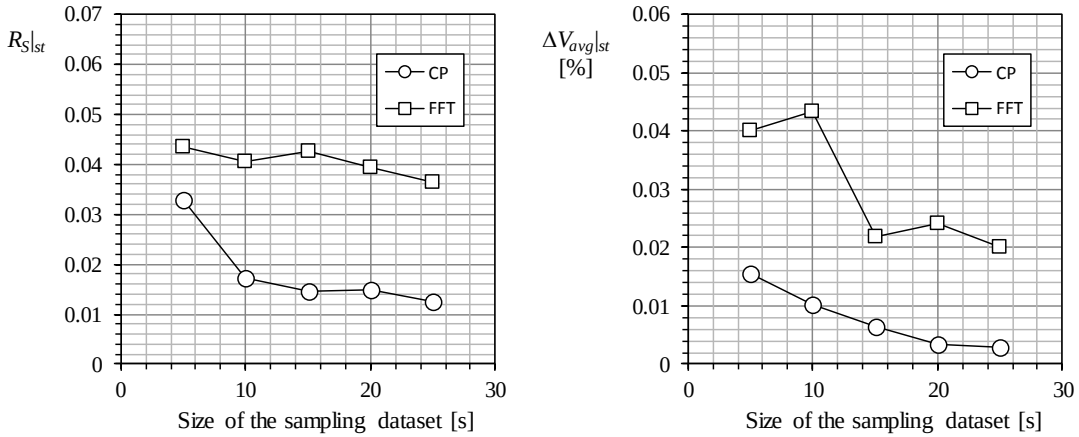

Figure 12. Anemometer-5. Stabilized values of the residuals, $R_S|_{st}$, and the wind speed error, $\Delta V_{avg}|_{st}$, in relation to the sampling dataset length.

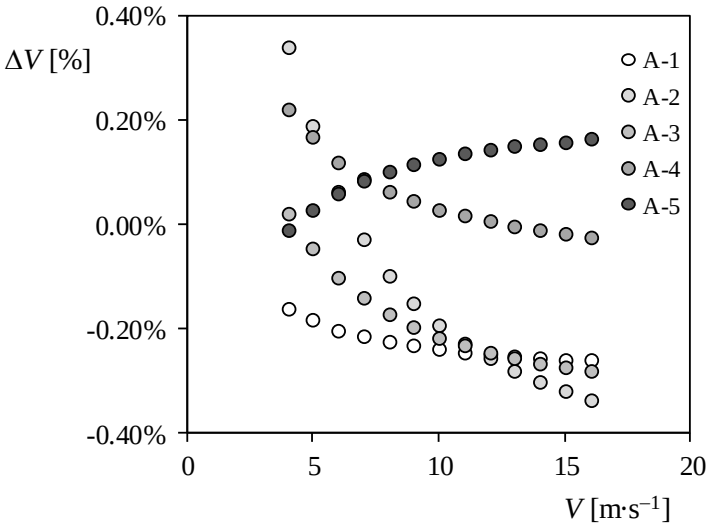

Figure 13. Percentage wind speed error in relation to the reference transfer function, ΔV, as a function of the wind speed, V. Data from calibrations based on FFT with regard to Anemometers 1 to 5 (A-1 to A-5) 25 kHz/25 seconds measurement datasets.

4 Conclusions

The aim of the present technical note is to analyze the effect of the sampling frequency, the length of the samples, and the procedure to obtain the output frequency (comparing CP and FFT) during cup anemometer calibration, on the accuracy of the transfer function. The most significant conclusions derived from the preset work are the following:

- Larger samples increase the accuracy of the transfer function. Nevertheless, it seems that this accuracy remains within a stabilized range for sample lengths larger than 20 s.
- The results suggest that sampling frequencies larger than 781.25 Hz are required to measure the output frequency of Thies Clima First-Class Advanced during a MEASNET calibration procedure. This requirement should change for other cup anemometers with different number of square pulses per turn (Thies Clima First-Class Advanced gives 37 pulses per turn whereas Vector Instruments A100 LK/LM gives 25).
- Counting pulses (CP) has proven to be the better way to extract the output frequency when compared to FFT, the error of calibrations based on the latter being within ±0.4% bracket (for enough large values of both the dataset and the measurement frequency).

Acknowledgments

The authors are indebted to Prof. Ángel Sanz-Andrés for his encouraging support regarding the research program on cup anemometers performance. The authors are truly indebted to the LAC-IDR/UPM staff for their constant support to this research.

References

[1] Lundquist J K and Bariteau L 2014 Dissipation of Turbulence in the Wake of a Wind Turbine *Boundary-Layer Meteorol.* **154** 229–41

[2] McCaffrey K, Quelet P T, Choukulkar A, Wilczak J M, Wolfe D E, Oncley S P, Alan Brewer W, Debnath M, Ashton R, Valerio Iungo G and Lundquist J K 2017 Identification of tower-wake distortions using sonic anemometer and lidar measurements *Atmos. Meas. Tech.* **10** 393–407

[3] Muñoz-Esparza D, Sharman R D and Lundquist J K 2017 Turbulent dissipation rate in the atmospheric boundary layer: observations and WRF mesoscale modeling during the XPIA field campaign *Mon. Weather Rev.* MWR-D-17-0186.1

[4] Bodini N, Lundquist J K and Newsom R K 2018 Estimation of turbulence dissipation rate and its variability from sonic anemometer and wind Doppler lidar during the XPIA field campaign *Atmos. Meas. Tech.* **11** 4291–308

[5] Muñoz-Esparza D and Sharman R 2018 An improved algorithm for low-level turbulence forecasting *J. Appl. Meteorol. Climatol.* **57** 1249–63

[6] Cutler N J, Outhred H R and MacGill I F 2012 Using nacelle-based wind speed observations to improve power curve modeling for wind power forecasting *Wind Energy* **15** 245–58

[7] Wagner R, Pedersen T F, Courtney M, Antoniou I, Davoust S and Rivera R L 2013 Power curve measurement with a nacelle mounted lidar *Wind Energy* **20** n/a-n/a

[8] Mikkelsen T, Angelou N, Hansen K, Sjöholm M, Harris M, Slinger C, Hadley P, Scullion R, Ellis G and Vives G 2013 A spinner-integrated wind lidar for enhanced wind turbine control *Wind Energy* **16** 625–43

[9] Pedersen T F, Demurtas G and Zahle F 2015 Calibration of a spinner anemometer for yaw misalignment measurements *Wind Energy* **18** 1933–52

[10] St. Martin C M, Lundquist J K, Clifton A, Poulos G S and Schreck S J 2016 Atmospheric turbulence affects wind turbine nacelle transfer functions *Wind Energy Sci. Discuss.* 1–22

[11] Demurtas G, Friis Pedersen T and Wagner R 2017 Nacelle power curve

measurement with spinner anemometer and uncertainty evaluation *Wind Energy Sci.* **2** 97–114

[12] Lang S and McKeogh E 2011 LIDAR and SODAR Measurements of Wind Speed and Direction in Upland Terrain for Wind Energy Purposes *Remote Sens.* **3** 1871–901

[13] Wagner R, Courtney M, Gottschall J and Lindelöw-Marsden P 2011 Accounting for the speed shear in wind turbine power performance measurement *Wind Energy* **14** 993–1004

[14] Bradley S 2013 Aspects of the Correlation between Sodar and Mast Instrument Winds *J. Atmos. Ocean. Technol.* **30** 2241–7

[15] Sanz Rodrigo J, Borbón Guillén F, Gómez Arranz P, Courtney M S, Wagner R and Dupont E 2013 Multi-site testing and evaluation of remote sensing instruments for wind energy applications *Renew. Energy* **53** 200–10

[16] Hasager C, Stein D, Courtney M, Peña A, Mikkelsen T, Stickland M and Oldroyd A 2013 Hub Height Ocean Winds over the North Sea Observed by the NORSEWInD Lidar Array: Measuring Techniques, Quality Control and Data Management *Remote Sens.* **5** 4280–303

[17] Suomi I and Vihma T 2018 Wind gust measurement techniques—From traditional anemometry to new possibilities *Sensors (Switzerland)* **18** 1–27

[18] Mikkelsen T 2014 Lidar-based Research and Innovation at DTU Wind Energy – a Review *J. Phys. Conf. Ser.* **524** 012007

[19] Frehlich R and Sharman R 2004 Estimates of Turbulence from Numerical Weather Prediction Model Output with Applications to Turbulence Diagnosis and Data Assimilation *Mon. Weather Rev.* **132** 2308–24

[20] Towers P and Jones B L 2016 Real-time wind field reconstruction from LiDAR measurements using a dynamic wind model and state estimation *Wind Energy* **19** 133–50

[21] Willis D J, Niezrecki C, Kuchma D, Hines E, Arwade S R, Barthelmie R J, DiPaola M, Drane P J, Hansen C J, Inalpolat M, Mack J H, Myers A T and Rotea M 2018 Wind energy research: State-of-the-art and future research directions *Renew. Energy* **125** 133–54

[22] Roibas-Millan E, Cubas J and Pindado S 2017 Studies on cup anemometer performances carried out at IDR/UPM Institute. Past and present research *Energies* **10** 1–17

[23] Pindado S, Vega E, Martínez A, Meseguer E, Franchini S and Pérez I 2011 Analysis of calibration results from cup and propeller anemometers. Influence on wind turbine Annual Energy Production (AEP) calculations *Wind Energy* **14** 119–32

[24] Pindado S, Barrero-Gil A and Sanz A 2012 Cup Anemometers' Loss of Performance Due to Ageing Processes, and Its Effect on Annual Energy Production (AEP) Estimates *Energies* **5** 1664–85

[25] Pindado S, Sanz A and Wery A 2012 Deviation of Cup and Propeller Anemometer Calibration Results with Air Density *Energies* **5** 683–701

[26] Vega E, Pindado S, Martínez A, Meseguer E and García L 2014 Anomaly detection on cup anemometers *Meas. Sci. Technol.* **25** 127002 (6pp)

[27] Wyngaard J C, Bauman J T and Lynch R A 1974 Cup anemometer dynamics *Flow Its Meas. Control Sci. Ind.* **1** 701–8

[28] Busch N E and Kristensen L 1976 Cup anemometer overspeeding *J. Appl. Meteorol.* **15** 1328–1332

[29] Wyngaard J C 1981 Cup, propeller, vane, and sonic anemometers in turbulence research *Annu. Rev. Fluid Mech.* **13** 399–423

[30] Westermann D 1996 Overspeeding - über das eigentümliche Tiefpaßverhalten von Schalensternanemometern (Overspeeding measurements of cup anemometers) *DEWI Mag.* **9** 56–63

[31] Kristensen L 2000 Measuring Higher-Order Moments with a Cup Anemometer *J. Atmos. Ocean. Technol.* **17** 1139–48

[32] Kristensen L, Jensen G, Hansen A and Kirkegaard P 2001 *Field Calibration of Cup Anemometers. Risø–R–1218(EN)* (Roskilde, Denmark)

[33] Pindado S, Cubas J and Sorribes-Palmer F 2015 On the harmonic analysis of cup anemometer rotation speed: A principle to monitor performance and maintenance status of rotating meteorological sensors *Measurement* **73** 401–418

[34] Martínez A, Vega E, Pindado S, Meseguer E and García L 2016 Deviations of cup anemometer rotational speed measurements due to steady state harmonic accelerations of the rotor *Measurement* **90** 483–90

[35] Vidal-Pardo A and Pindado S 2018 Design and Development of a 5-Channel Arduino-Based Data Acquisition System (ABDAS) for Experimental Aerodynamics Research *Sensors* **18** 1–20

[36] Nyquist H 1928 Certain Topics in Telegraph Transmission Theory *Trans. Am. Inst. Electr. Eng.* **47** 617–44